EUROPEAN ORGANIZATION FOR NUCLEAR RESEARCH

CERN/EP 83-31
(CERN/DD 83-1)
24 February 1982

IMPLEMENTATION AND PERFORMANCE OF THE OPTICAL FIDUCIAL VOLUME TRIGGER USED WITH THE RAPID CYCLING BUBBLE CHAMBER

H. Anders, P. Bähler, D.A. Jacobs, K.E. Johansson,
B.J. Pijlgroms and R. Zurbuchen
CERN, Geneva, Switzerland

ABSTRACT

A description is given of the software algorithms used for the Optical Fiducial Volume Trigger system (OFVT) and the implementation on-line. The OFVT system has the purpose of enhancing the efficiency of the trigger system for the Rapid Cycling Bubble Chamber (RCBC) of the European Hybrid Spectrometer (EHS). One obtains an efficiency for good events of 80-90% and a rejection efficiency for events outside the bubble chamber fiducial volume of 60-70%. With the use of OFVT the fraction of pictures containing a useful event rises from 30% to 55%.

Submitted to Nuclear Instruments and Methods

1403P/BJP/mk

1. INTRODUCTION

The Optical Fiducial Volume Trigger (OFVT) [1,2] is intended to be used with the Rapid Cycling Bubble Chamber (RCBC) in the European Hybrid Spectrometer (EHS) [3]. The trigger for the EHS experiments usually only demands that an interaction has occurred in the bubble chamber or in its immediate surrounding. The probability that an interaction will occur in the useful central part, the fiducial volume, is relatively small since the bubble chamber windows as well as the bubble chamber liquid close to the windows give rise to a large fraction of unusable interactions. In fact 60-70% of the interactions occur outside the fiducial volume and are not used for physics. It is consequently desirable to reject these events in as early a stage as possible, and this is the aim of the Optical Fiducial Volume Trigger.

The OFVT is intended to work as an on-line trigger. For the first experiment with the RCBC (the NA23 experiment [4]) data were taken with the aim of determining the OFVT efficiency and optimizing the trigger algorithm off-line. As a second phase the OFVT was implemented on-line to be used for a second NA23 data taking run and for other RCBC experiments.

In bubble chamber experiments very often the data taking rate is limited by the maximum frequency of the cameras. It is therefore of interest to avoid taking a picture when the interaction has occurred outside the fiducial volume. It is then possible to increase the sensitivity of the experiment for a given running time (or decrease the running time for a given sensitivity). If the experiment is not limited by the camera frequency, then the effect of an efficient fiducial volume trigger is mainly to reduce the number of pictures taken and the associated amount of scanning of the pictures.

In sect. 2 the OFVT hardware and the on-line implementation is described, sect. 3 treats the OFVT trigger algorithm and sect. 4 describes the performance. In sect. 5 the systematic losses are described and sect. 6 contains the summary.

2. THE OFVT HARDWARE AND THE ON-LINE IMPLEMENTATION

2.1 The principle of the OFVT

The principle of the OFVT hardware is the following (fig. 1). The image of two bands at right angles to the particle beam, one on each side of the fiducial volume are projected onto two diode arrays. Each array is formed by 1872 light sensitive diodes which are read out sequentially. On the array output signals, tracks crossing the array areas appear as pulses from which the track positions in the beam plane can be calculated. The track coordinates are used to determine if the interaction occurred in the fiducial volume.

The logic relies on a practically perfect track detection efficiency. This is assured by averaging the tracks over a sufficient length in order to minimise the local density variations caused by the fact that the tracks are composed by chains of bubbles with interstices between them. The averaging is achieved by using long diode cells combined with an anamorphic imaging by cylindrical lenses placed in front of each array. The area in the chamber beam plane covered by each array is 150 x 11mm^2. One diode cell covers an area 11 mm along the beam and 80 µm wide. The distance between the two bands in the bubble chamber corresponds to 600 mm.

The OFVT flash is triggered 300 µs after an interaction. The flash delay and duration, the signal read out and the decision logic takes about 900 µs. This leaves plenty of time for vetoing the trigger of the photographic cameras occuring 1.5 ms after the interaction.

Fig. 1 shows the position of the diode arrays and their projection in the bubble chamber. Also shown are the relative positions of the upstream wire chambers U1 and U3 which are used to calculate the position in the bubble chamber of the triggering beam track.

2.2 The OFVT camera and the read-out electronics

The OFVT camera (fig. 2) contains the optics, the flash tube and the diode arrays together with parts of the read out electronics. The camera is mounted on the magnet structure and looks into the bubble chamber through one of the optical windows. Band-pass filtering the flash light from 600 nm to 700 nm prevents exposure of the RCBC camera film and limits the chromatic aberration.

Following an exposure the diode information is read out at a rate of 10 MHz and the track coordinates are extracted by the read-out electronics (fig. 2). The electronics includes a background subtraction feature which supresses any constant structure in the optical and the array signals. This leads to a considerable improvement of the track detection efficiency. For this purpose background information is read out from time to time and stored in the background memory. After adequate software treatment the modified background is subtracted from the array signals for every read out cycle. The track detection circuits use a double delay line discriminator. The track position digitizer makes use of a synchronous position counter for digitizing the leading and the trailing edge of each track pulse from which the track centres and widths are calculated. All track coordinates of a read out are stored in the track position memory.

More details about the OFVT hardware are found in ref. [5].

2.3 The incorporation of the OFVT into the EHS data acquisition system

The OFVT is interfaced to the EHS data acquisition computer through ESOP [6], a fast microprocessor. The main task of this microprocessor consists of generating an 'accept' or a 'reject' signal for the trigger electronics according to the trigger algorithm (figs 3, 4) which is described in chapter 3. The trigger electronics then generates either an 'abort' signal which reinitializes all detectors of the spectrometer or a trigger signal which triggers the bubble chamber camera system and starts the read out cycle in the NORD-100 data acquisition computer. During this read out cycle, ESOP is also used for passing the OFVT track information and its decision to the NORD-100. The OFVT data as well as the data of the other detectors are written onto tape for off-line analysis.

For trigger set up and monitoring, the NORD-100 is able to dump events and to generate diode maps as well as histograms of the multiplicity and the cluster width. For the trigger algorithm ESOP uses also the data of the two Multi Wire Proportional Chambers (MWPC) U1 and U3 (fig. 1) in order to predict the position of the triggering beam track in the diode arrays. These data pass via a buffer memory (fig. 2) which is accessible from both the NORD-100 and ESOP.

ESOP has access to the OFVT background memory, the content of which can be investigated and modified. For example the signal due to the reference wire (a wire of 150 µm diameter which is stretched in the RCBC beam plane parallel to the beam tracks serves as a spatial reference and for monitoring purposes), has to be removed otherwise it would be eliminated as background.

Since OFVT is working in a "production environment" all actions like measuring the background, reading it out, modifying and loading it are done without interfering with the data taking. This is achieved by synchronizing all critical actions with respect to the beam and trigger timing. The timing diagram in fig. 5 shows the interaction of the OFVT system and the EHS data aquisition system. The data acquisition cycle is started by a spill prewarning pulse which in the NORD-100 activates initialisation routines for the OFVT and the different detectors. The MWPC intialisation routine also activates ESOP to initialize the buffer memory for the MWPC data and to wait for the "data ready" signal. After receiving the MWPC data, ESOP prepares them for transfer to the NORD-100 and calculates the beam prediction for the first diode array which needs only the information of U1 and U3. After receiving the data from OFVT the second part of the veto routine is executed to produce a decision.

3. THE OFVT TRIGGER ALGORITHM

The OFVT trigger algorithm was designed and tested off-line using the data of the NA23 experiment using a 360 GeV/c proton beam. As only a limited amount of time is available for decision making on-line, it was desirable to find a simple but nevertheless accurate algorithm.

Fig. 3 shows a flow diagram of the veto routine in ESOP. First the MWPC data of U1 and U3 is read out and tested for legality. From these data the beam position in array A1 is predicted. If there are not too many beam tracks seen in A1, the hit in A1 is in its turn used to calculate a prediction in array A2. A detailed description of this calculation is given in the Appendix.

Once the predicted beam positions are known, the decision tree shown in fig. 4 is entered. For each branch in the tree a condition, usually depending on a certain parameter, is tested after which an exit from the tree may occur. The order in which the conditions are tested was chosen in such a way that it causes the minimal amount of biases for the possible physics experiments. The parameter values were optimized off-line to give the best performance.

Branch 1

If the beam particle is not detected in array A1 within a certain window around the predicted beam position, it is very likely that the interaction occurred upstream of A1. In this case the event is rejected. The size of the window should be at least 2-3 standard deviations of the residuals between predicted and actually found beam positions. If the window is chosen much larger, the probability of picking up other beam tracks lying nearby increases.

Branch 2

If in array A1 the measured track width is much larger than average, it is very likely that the interaction took place upstream but very close to array A1 so that the secondary tracks were not resolved. The cut-off parameter depends on the bubble size and therefore on the flash delay. However, in practice this test is relatively unimportant and could be left out of the tree without affecting the performance substantially.

Branch 3

If the number of tracks in array A2 is larger than in array A1, it is very likely that the interaction took place inside the fiducial volume. The event is then accepted. The multiplicity increase should however be counted locally, i.e. within a certain window around the beam predictions. Of the two tested windows of 6 and 12 mm, the larger one gave the better results.

Branch 4

If there is no multiplicity increase, but the beam is not present within a small window around the predicted position in array A2, the event is accepted. As in branch 1 the window size should be 2-3 standard deviations of the residual distribution in array A2. It is very important

that this window is as small as possible in order not to lose too many small angle events such as target fragmentation, leading particle effect or elastic scattering. As described in the Appendix it is possible to obtain a prediction for array A2 that is an order of magnitude more precise than for array A1.

Branch 5

If the number of tracks decreases from array A1 to array A2 it is very likely that the interaction occurred upstream, for instance, in the bubble chamber window. This test should occur after branch 4 in order not to lose large angle events like inelastic two-prong events or zero-prong events in case of annihilation interactions.

Branch 6

A large track width in array A2 indicates that the interaction occurred close to and upstream of array A2. This event configuration is accepted but this branch is relatively unimportant.

Branch 7

The events that reach this last branch are mainly through-going beam tracks that interact downstream of the fiducial volume. This configuration is usually rejected. However, a relatively small number of small angle events that were not detected in branch 4 would also be rejected at the same time. Therefore, for the NA23 experiment this category of events was partly recuperated by combining the OFVT information with the information from the main trigger.

4. THE PERFORMANCE OF THE OFVT

The performance of the OFVT depends both on the efficiency to detect a track and on the correct interpretation of the pattern of track coordinates.

4.1 Determination of the detection efficiency

Examining the corresponding pictures on a scanning table, it was checked whether the two diode arrays had registered correctly the crossing of about 550 beam tracks. No track was missed which means that the track

detection efficiency was 100%. This investigation was done using OFVT data which were taken with a flash delay of 300 μs. For this delay the corresponding bubble size is typically 85 μm. At longer delays the bubbles have larger diameter and therefore the tracks should be detected even more safely.

4.2 The mechanical stability of the OFVT

The mechanical stability of the OFVT hardware relative to the reference wire was examined by making plots of the wire positions detected by the OFVT arrays. For a period of several hours the wire positions stayed constant within 40 μm. Repeating this test one day later showed that the long term drift also remained within 40 μm.

4.3 The performance of the OFVT logic

Table 1 shows the results of applying the ESOP algorithm to three samples of events taken under different conditions. In the ideal case all the interactions outside the fiducial volume should occur on the reject lines and all those inside should occur on the accept lines.

In table 1 are also given the frequencies of the most important error conditions. If no hit is found in one of the upstream wire chambers, no predictions can be calculated. If more than one hit is found per wire chamber the predictions become ambiguous. In these cases the beam predictions are not calculated. If the number of beam tracks in the bubble chamber is too big, the time needed for ESOP to make a decision becomes too long. Besides this, on the scanning table it was found that an event seen in such a picture was in most cases practically unmeasurable. To avoid the possibility of bias, all error conditions mentioned above resulted in an accept of the event. However, as is demonstrated below, a better efficiency is obtained if events with these error conditions are rejected.

Table 2 shows the most important numbers derived from the results in table 1. Note the importance of the number of beam tracks per picture shown in the first line. If this parameter is increased one expects that the confusion increases and that the performance may decrease.

In the upper block of table 2 the situation is given without using OFVT. A picture containing an event in the fiducial volume is called a good picture, otherwise it is called a bad picture. The film efficiency is defined as the fraction of good pictures on the film.

The second block of the table shows the results using OFVT with all error conditions resulting in an accept. The acceptance is defined as the fraction of good pictures accepted by OFVT and the rejectance means the efficiency to reject bad pictures. One sees that the acceptance is quite good; it is on the average 85% and nearly independent of the number of beam particles. On the other hand, the rejectance drops considerably with increasing beam density and varies between 20 and 70%. The film and scan cost number is defined as the fraction of film needed with OFVT to obtain the same number of good pictures as without using OFVT. It is clear that this quantity increases with decreasing rejectance. In the best case the film and scan cost reduces to about 60% using OFVT.

The third block in table 2 shows the situation when using the ESOP algorithm where events with error conditions are suppressed. In this case the acceptance decreases a few per cent but the rejectance rises considerably which results in a high film efficiency and a low film cost. It is striking to see that the film efficiency seems to reach a constant value of about 55%, independently of the number of beam particles per picture.

From table 2 one can see that the best performance is achieved using the option where one rejects the events with incomplete or too much data. In this case the acceptance is typically 80% and the rejectance varies between 60 and 70% depending on the beam intensity.

In table 3 the performance of the OFVT is shown when the possible target fragmentation events that normally are rejected in branch 7 of the decision tree are recuperated on-line. This recuperation is done by combining the ESOP signal with a signal of the main trigger electronics when an exit occurs in branch 7. Although in this branch 50% of the good events are saved by this method, also 50% of the bad pictures are accepted. Since the first category is much less numerous than the latter one, the acceptance of useful events increases somewhat while the

rejectance of useless events decreases considerably, as is seen by comparing tables 2 and 3. On the whole the performance of the OFVT degrades.

5. THE SYSTEMATIC LOSSES AND THE PROPOSED CORRECTION METHOD

The acceptances for the different topologies for the NA23 experiment are given in table 4 (off-line results with the error conditions accepted). Averaged over all topologies the acceptance is 83 ± 2%. However, if one excludes the 2-prong events from the sample, the acceptance is 89 ± 2% and is roughly independent of the topology. For the 2-prong events, containing a large fraction of small angle elastic reactions, the acceptance is only 49 ± 8%. For this channel the angle below which no events can be found equals $\theta \simeq 0.3$ mrad corresponding to a t cut around 0.015 $(GeV/c)^2$. The loss of inelastic events of 11 ± 2% is a sum of systematic and random losses. The random losses are caused by a pick-up of other nearby beam tracks or confusion with the wire in the bubble chamber.

Fig. 6 shows the distributions of the vertex x-position along the beam direction in the OFVT fiducial volume for the accepted and the rejected events respectively. Within the available statistics the distributions are reasonably flat, but there seems to be a slight tendency to lose more events near the end of the fiducial volume.

The systematic losses can easily be corrected for off-line by using the principle of weighting. Since the losses are completely defined by the geometry of the event and the trigger hardware, one can calculate for every event found the probability that it would have been lost had it occurred at another position or with a different orientation in the fiducial volume. This probability defines for every particular event a weight that should be assigned to the event in order to get the correct cross sections. A test of this weighting procedure is to require a constant weighted number of events if one or more of the geometrical parameters are varied. The very small angle events that are not detected at all cannot be recovered by weighting but should be corrected for by upgrading of a small unbiassed data sample. A more detailed description of similar methods can be found in ref. [7].

6. SUMMARY

In this paper we described the software algorithm for the Optical Fiducial Volume Trigger system (OFVT), its implementation on-line and its performance. From the analysis of the opto-electronic system we find that the mechanical stability of the OFVT is equal to 40 μm in space in the bubble chamber, which equals half a physical least count of the photo-diode arrays. For the detection of beam tracks we find that the efficiency is 100% for an OFVT flash delay of 300 μs or more.

The ESOP trigger algorithm was determined in such a way that the systematic losses are minimal for all possible physics experiments. The calibration of the system is done on-line. The performance was tested for different data taking conditions and for a varying number of beam tracks per picture. The acceptance of useful interactions ranges between 80 and 90% and the efficiency to reject useless interactions reaches 60 to 70%. In the best cases the fraction of good events increases from 30% to 55-60% when the OFVT is used. The systematic losses are low and are mainly found among events with only one forward going small angle track. A method is indicated to correct for these losses off-line.

Acknowledgements

The authors would like to thank B. Powell, Ch. Roos, R. Settles and A. Subramanian who have taken part in the first stages of the project, and also G. Neuhofer and J. Hrubec for their help with the interfacing of OFVT with the main trigger electronics. In addition we thank L. Montanet for his continuous interest and support for the project.

APPENDIX

CALCULATION OF THE PREDICTIONS AND THE CALIBRATION

It is important to be able to determine and modify on-line the parameters that are used to calculate the predictions for the arrays A1 and A2 as the data taking conditions could change during the run. The predictions are calculated from the upstream wire chambers U1 and U3. From U1 only one plane is used and from U3 two crossed planes are used. All planes have 2 mm wire spacing. If one neglects the influence of the magnetic field a first order approximation for the predictions can be obtained from a linear extrapolation

$$y_{PR1,2} = a_0 + a_1 \cdot y_{U1} + a_2 \cdot y_{U3} \qquad (1)$$

in which y_{U1} and y_{U3} represent the hits in the wire chambers, $y_{PR1,2}$ the predictions for array A1 and array A2 and a_0, a_1 and a_2 are coefficients which are different for the two arrays.

A second order approximation for the prediction in array A2 can be obtained by adding to the predicted position the residual $\delta y_1 = y_{A1} - y_{PR1}$ between the prediction y_{PR1} and the position y_{A1} actually found in array A1 (fig. 7). The formula for array A2 now becomes

$$y'_{PR2} = b_0 + b_1 \cdot y_{U1} + b_2 \cdot y_{U3} + y_{A1} \,. \qquad (2)$$

A better third order approximation can be obtained by also making a correction for the angle under which the beam track crosses the chambers and arrays (fig. 7). In this case the prediction for array A2 becomes

$$y''_{PR2} = c_0 + c_1 \cdot y_{U1} + c_2 \cdot y_{A1} \qquad (3)$$

in which the term with y_{U3} is missing.

A first approximation for the coefficients can be obtained from the survey data. These then require refinement by calibration. It was found that, for this correction and that needed for the magnetic field, a linear transformation of the uncorrected formula was sufficient, leading to

$$y_{PR}^{c} = d_0 + d_1 \cdot y_{PR} \qquad (4)$$

in which y_{PR}^{c} is the corrected prediction and d_0, d_1 are the calibration coefficients. Substitution of eqs (1), (2) or (3) into eq. (4) leads then simply to new values of the constants a_i, b_i or c_i. An iterative process to calibrate the constants d_0 and d_1 is as follows. As starting values one sets $d_0 = 0$ and $d_1 = 1$ (no correction). Then one plots for each array the residuals δy as a function of the track position y_A. In first order approximation this yields a linear relation

$$\delta y = y_A - y_{PR} \simeq \alpha + \beta \cdot y_A \quad . \qquad (5)$$

If the values of d_0 and d_1 were correct this would imply that the fitted values for α and β are both zero. Therefore a better estimate for d_0 and d_1 is obtained by requiring that both α and β become zero. The new estimates are then

$$d_0' = \frac{\alpha + d_0}{1 - \beta} \quad \text{and} \quad d_1' = \frac{d_1}{1 - \beta} \quad . \qquad (6)$$

If the old values of d_i are close to the correct values d_i' this procedure is in principle a single step adaptive process. However, if the old values d_i differ significantly from the correct values, spurious tracks not belonging to the predicted tracks may be picked up. In that case several (in practice 4 to 5) iterations may be needed. For all iterations the same data sample consisting of approximately 500 events can be used. The complete calibration procedure can be done in about half an hour.

The RMS values of the residuals after calibration are given in table 5 for the off-line simulated and on-line results. The numbers quoted in the column "off-line, best approximation" correspond to the obtained off-line values where all wire chamber planes are used (5 planes of each chamber). The apparant positions at which the arrays see the tracks are corrected for the OFVT viewing angles and the corrections for magnetic field are made by a high order polynomial.

REFERENCES

[1] H. Anders, B. Powell, Ch. Roos and R. Settles, On-line readout of the optical picture of the Rapid Cycling Bubble Chamber of EHS, EHS Workshop held in Vezelay 26-28 October 1977, CERN/EP/EHS/PH 77-5, page 12.

[2] H. Anders, The optical fiducial volume trigger for RCBC, IInd Vezelay workshop on EHS, Vezelay, 2-5 March 1980, CERN/EP/EHS/PH 80-2, page 103.

[3] W. Allison et al., Study of multihadron events involving identified particles in high energy interactions, CERN/SPSC/75-15.

[4] A. Bergier et al., Study of diffractive dissociation especially into strange and charm particles, CERN/SPSC/80-53.

[5] H. Anders, J. Antonsen, R.E.S. Berglund, G. Channel, J. Oropesa, L. Sohet and R. Zurbuchen, The hardware design of the Optical Fiducial Volume Trigger for the Rapid Cycling Bubble Chamber of EHS, CERN/DD/83/2, to be submitted to Nucl. Instr. and Methods.

[6] D.A. Jacobs, Computer Phys. Comm. 26 (1982) 69.

[7] B.J. Pijlgroms, Thesis (1982), NIKHEF-H, Amsterdam.

TABLE CAPTIONS

Table 1 The OFVT decision tree as used by ESOP and the number of events inside and outside the fiducial volume for the three different experiments.

Table 2 OFVT efficiencies under different conditions. The features are described in the text.

Table 3 OFVT efficiencies when recuperating on-line a part of the "possible target fragmentation" events at 360 GeV/c. The features have the same meaning as in table 2.

Table 4 Topological breakdown of the losses of good events caused by OFVT for the NA23 experiment.

Table 5 The RMS values of the residuals between predicted and found beam positions for different methods and orders of approximation.

TABLE 1

ESOP branch	ESOP decision	NA23 360 GeV/c low intensity inside	NA23 360 GeV/c low intensity outside	NA23 360 GeV/c high intensity inside	NA23 360 GeV/c high intensity outside	NA22 250 GeV/c medium intensity inside	NA22 250 GeV/c medium intensity outside
1 no beam in array 1	Reject	30	64	0	3	0	16
2 large track width in array 1	Reject	8	46	0	2	1	4
3 local multiplicity increase	Accept	369	120	66	41	136	92
4 no beam in array 2	Accept	76	244	9	13	38	65
5 multiplicity decrease	Reject	7	99	8	28	19	69
6 large track width in array 2	Accept	3	2	0	0	1	0
7 through going beam	Reject	58	620	14	42	13	46
no hit found in MWPC plane	Error	-	-	0	1	0	4
more than one hit found in MWPC	Error	62	201	21	60	29	67
more than 25 tracks seen in OFVT	Error	-	-	55	162	4	12
	Total	613	1396	173	352	241	375

TABLE 2

	NA23 360 GeV/c low intensity	NA23 360 GeV/c high intensity	NA22 250 GeV/c medium intensity
Beams per picture	5.4	13.9	9.1
without OFVT			
good pictures	613	173	241
bad pictures	1396	352	375
film efficiency	31%	33%	39%
with OFVT (decision tree and accept of errors)			
good pictures	510	151	208
bad pictures	567	277	240
acceptance	83%	87%	86%
rejectance	59%	21%	36%
film efficiency	47%	35%	46%
film and scan cost	64%	93%	84%
with OFVT (decision tree and reject of errors)			
good pictures	448	75	175
bad pictures	366	54	157
acceptance	81%	77%	84%
rejectance	70%	58%	46%
film efficiency	55%	58%	53%
film and scan cost	57%	74%	74%

TABLE 3

	NA23 360 GeV/c low intensity	NA23 360 GeV/c high intensity
with OFVT (decision tree and accept of errors)		
good pictures	539	158
bad pictures	862	299
acceptance	88%	91%
rejectance	38%	15%
film efficiency	38%	35%
film and scan cost	79%	95%
with full OFVT (decision tree and reject of errors)		
good pictures	477	82
bad pictures	661	76
acceptance	87%	85%
rejectance	45%	41%
film efficiency	42%	52%
film and scan cost	75%	83%

TABLE 4

Topology	Events	Lost	Acceptance
All	613	103	83 ± 2%
≥ 4	525	58	89 ± 2%
2	88	45	49 ± 8%
4	73	13	82 ± 5%
6	83	11	87 ± 4%
8	82	7	91 ± 3%
10	94	9	90 ± 3%
12	64	5	92 ± 3%
14	49	5	90 ± 4%
16	37	4	89 ± 5%
18	19	2	89 ± 7%
≥ 20	24	2	92 ± 6%

TABLE 5

	Off-line	Off-line, (feasable on-line)			On-line
	best approx.	first order approx.	second order approx.	third order approx.	third order approx.
Array 1	180 μm	375 μm	375 μm	375 μm	533 μm
Array 2	31 μm	410 μm	155 μm	92 μm	55 μm

FIGURE CAPTIONS

Fig. 1 The principle of the OFVT. Three different interactions are schematically indicated two of which should be rejected. A1 and A2 are the bands in the bubble chamber projected onto the light sensitive diode arrays. The reference wire in the bubble chamber is also shown.

Fig. 2 Block diagram of the OFVT and wire chamber electronics.

Fig. 3 The flow diagram of the ESOP veto routine.

Fig. 4 The OFVT trigger algorithm in ESOP. The parameter values used are indicated in the figure.

Fig. 5 The interaction between ESOP and the NORD-100 data acquisition computer.

Fig. 6 The vertex position x-distribution along the beam direction of the accepted (a) and the rejected (b) events in the fiducial volume.

Fig. 7 The calculations of the predictions for the OFVT arrays A1 and A2. The full line represents the beam track and the crosses represent the actual hits in U1, U3, A1 and A2. The dashed lines indicate how the different predictions are obtained.

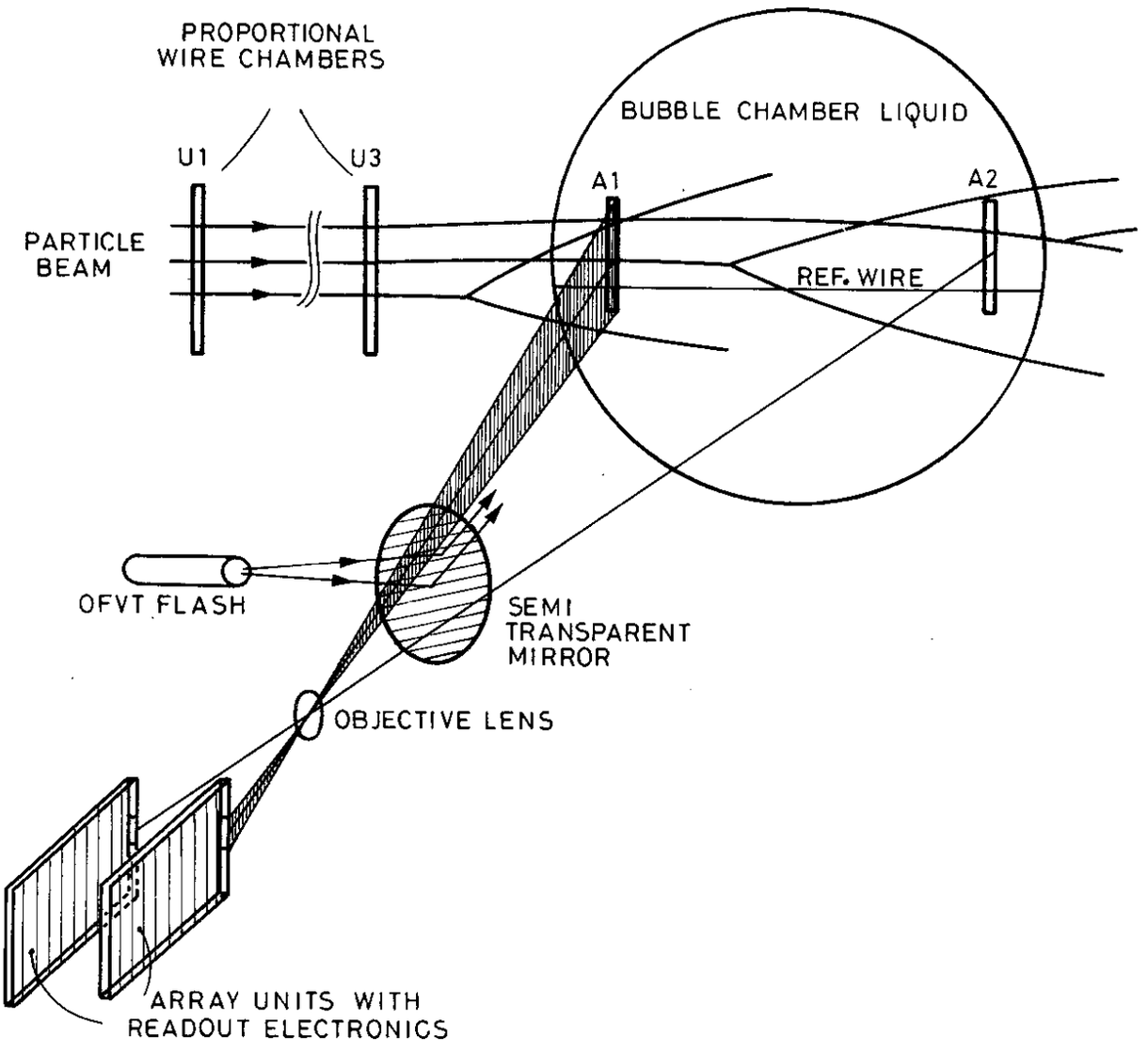

FIG. 1 THE BASIC PRINCIPLE OF THE OFVT

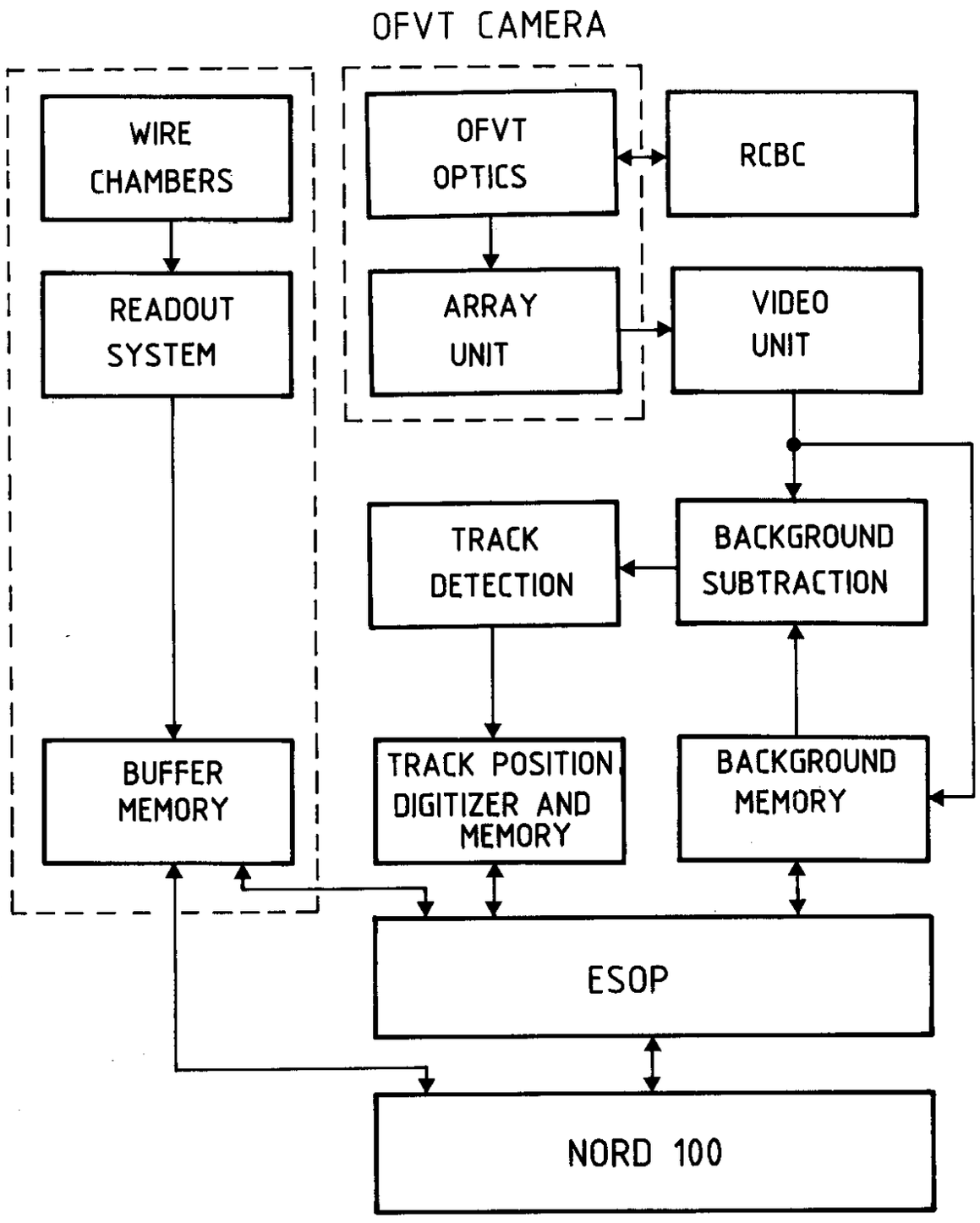

FIG. 2 OFVT AND WIRE CHAMBER ELECTRONICS BLOCK DIAGRAM

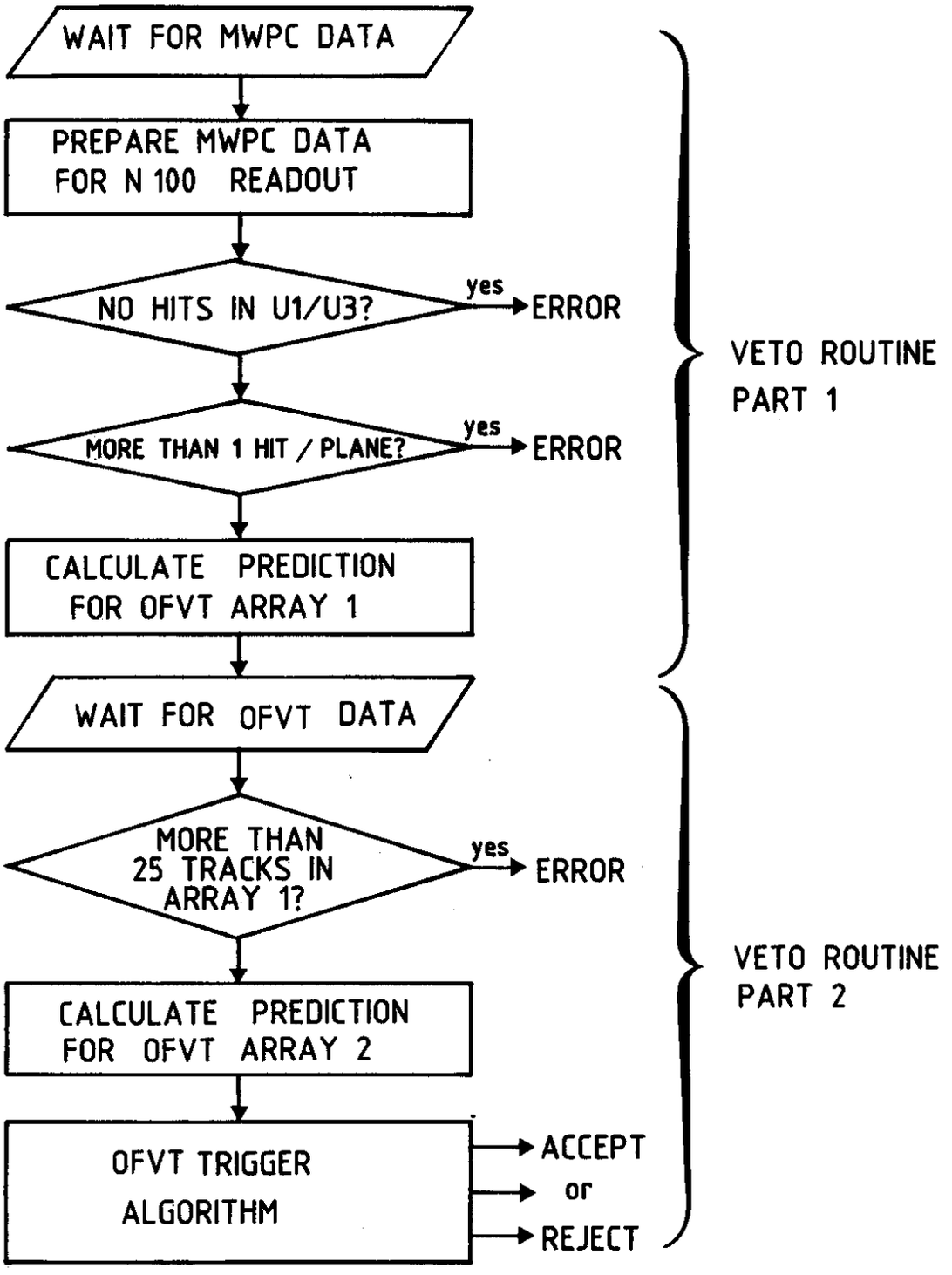

FIG. 3 FLOW DIAGRAM OF ESOP's VETO ROUTINE

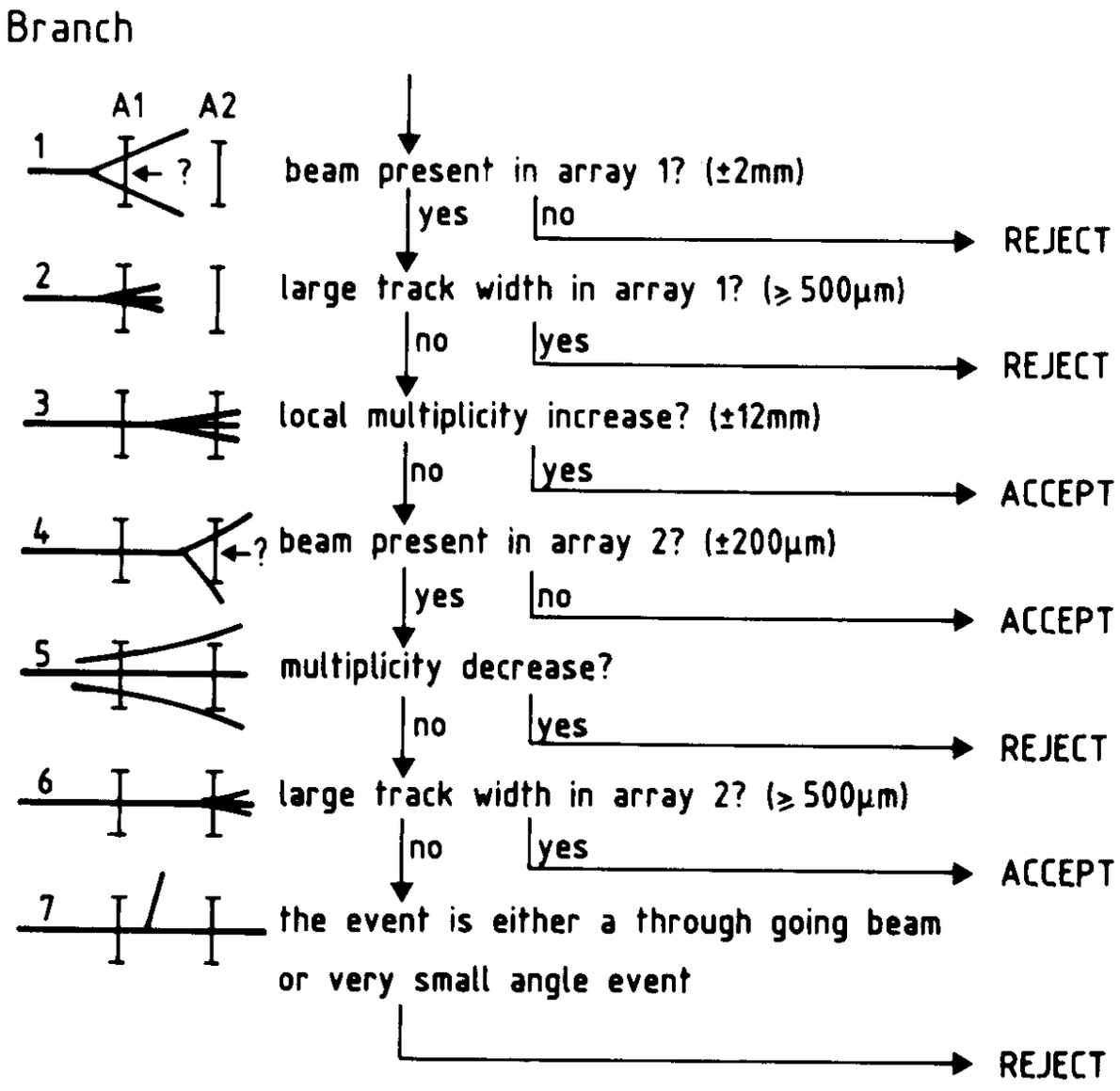

FIG. 4 The OFVT trigger algorithm in ESOP. The parameter values used are indicated in the figure

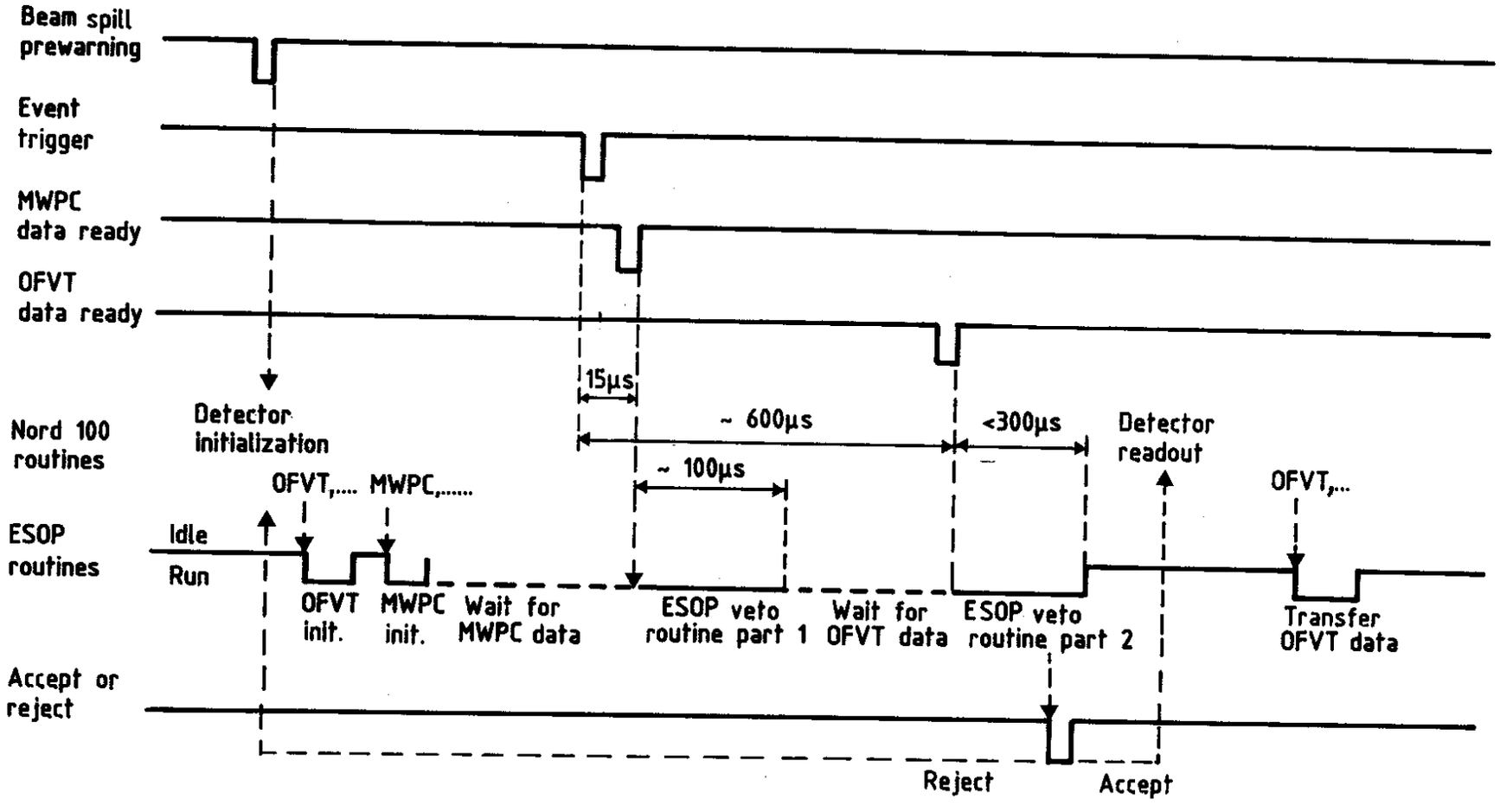

FIG. 5 Interaction between ESOP and the data acquisition computer..

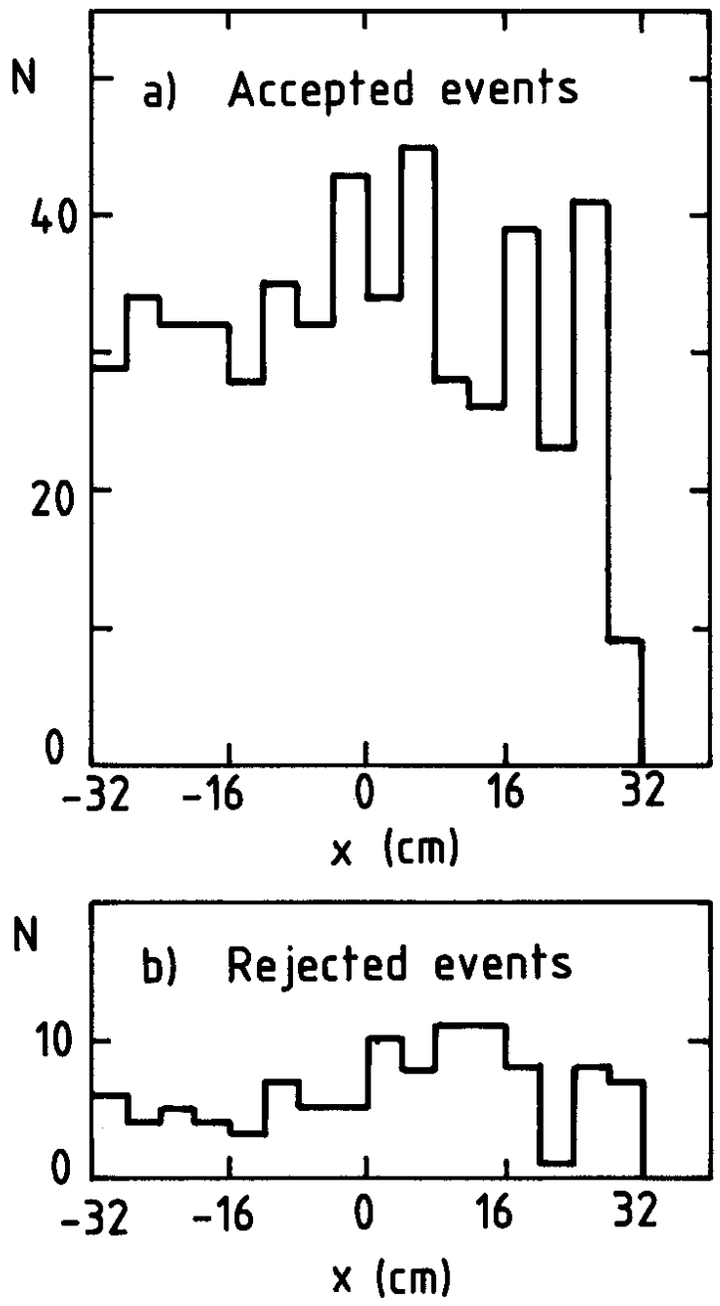
N
a) Accepted events
40
20
0
-32
-16
0
16
32
x (cm)
N
b) Rejected events
10
0
-32
-16
0
16
32
x (cm)

FIG. 6

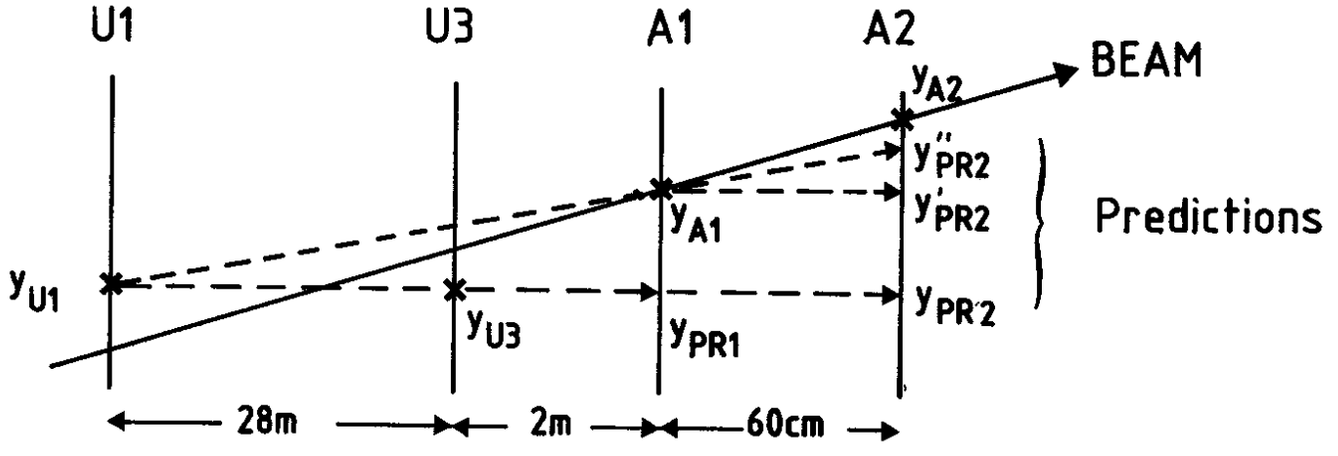
U1
U3
A1
A2
BEAM
y_{A2}
y''_{PR2}
y'_{PR2}
y_{A1}
Predictions
y_{U1}
y_{U3}
y_{PR1}
y_{PR2}
28m
2m
60cm

FIG. 7